High-pressure structures and vibrational spectra of barium fluoride: Results obtained under nearly hydrostatic conditions

Jesse S. Smith,[1,*] Serge Desgreniers,[1] John S. Tse,[2] Jian Sun,[3,†] Dennis D. Klug,[3] and Yasuo Ohishi[4]
[1]*Laboratoire de physique des solides denses, Department of Physics, University of Ottawa, Ottawa, Ontario, Canada K1N 6N5*
[2]*Department of Physics and Engineering Physics, University of Saskatchewan, Saskatoon, Saskatchewan, Canada S7N 5E2*
[3]*Steacie Institute for Molecular Sciences, National Research Council of Canada, Ottawa, Ontario, Canada K1A 0R6*
[4]*Materials Science Division, Japan Synchrotron Radiation Research Institute (JASRI), SPring-8, Sayo, Hyogo 679-5198, Japan*
(Received 22 November 2008; published 6 April 2009)

Powder x-ray diffraction and Raman spectroscopy experiments, together with first-principles calculations, have been carried out to corroborate and clarify the pressure-dependent structural evolution of barium fluoride. X-ray diffraction experiments were performed both with and without a pressure-transmitting medium. The latter serve to reproduce past experimental results, while the former show a marked difference. Specifically, the experiments employing helium as a pressure-transmitting medium yield observed relative intensities and volume compression consistent with the proposed Ni_2In structure of barium fluoride at pressures greater than 14 GPa. The Raman spectroscopy measurements corroborate the proposed Ni_2In structure, as the spectra exhibit the two modes expected for the high-pressure phase. The experiments also demonstrate that barium fluoride remains an insulator up to at least 77 GPa, and the results of first-principles calculations suggest that a subsequent insulator-metal transition may not be expected well into the megabar regime.

DOI: 10.1103/PhysRevB.79.134104 PACS number(s): 61.50.Ks, 62.50.−p, 78.30.−j

I. INTRODUCTION

The pressure-dependent properties of ionic AX_2 compounds are of considerable interest in a number of applied and fundamental respects. For example, many of the oxides are relevant in various industrial[1] and geological[2] contexts, and several of the hydrides have been examined as possible systems for hydrogen storage and exchange[3] and for elucidating hydrogen lattice dynamics.[4] Furthermore, as relatively simple binary compounds, many AX_2 compounds are well suited to powerful computational methods over a broad range of thermodynamic conditions. BaF_2 has played an important role in the study of these materials. It served as the first explicit example of a pressure-induced structural phase transition for which the high-pressure structure is characterized by a cation coordination number of 11 (Ref. 5) and both computational[6] and experimental[7] studies have predicted an insulator-metal transition at the relatively modest pressures (modest with respect to the current limits of static high-pressure techniques) of 33 and 87 GPa, respectively.

At ambient conditions, BaF_2 adopts the cubic fluorite structure ($Fm3\text{-}m$, Z=4) (Ref. 8). A pressure-induced phase transition at approximately 3 GPa was first identified by Smith and Chen[9] and shortly thereafter confirmed and clarified by Seifert,[10] who proposed the cotunnite structure (orthorhombic, $Pnam$, Z=4) for the high-pressure phase. This proposed structure was later corroborated by the Raman spectroscopy measurements of Kessler *et al.*,[11] carried out at low temperature (77 K) and high pressure (up to approximately 3 GPa).

Upon undertaking powder x-ray and neutron-diffraction studies, Leger *et al.*[5] reported they could expect, based on their previous work,[12] that at yet higher pressures BaF_2 would adopt a monoclinic structure. This would follow the structural progression cubic→orthorhombic→monoclinic which in turn would be characterized by a progression in the cation coordination number 8→9→10. Instead they found upon increasing pressure that at approximately 15 GPa, BaF_2 undergoes a first-order structural phase transition with a proposed Ni_2In structure (hexagonal, $P6_3/mmc$, Z=2). As mentioned above, this was the first explicit example of cation coordination number 11 among AX_2 compounds, although Leger *et al.* noted that the structure proposed by Lebech *et al.* for YbH_2 at pressures greater than approximately 14.3 GPa (Ref. 13) is the same as that proposed for BaF_2 at pressures greater than approximately 15 GPa, and would therefore also constitute an example of cation coordination number 11 in ionic AX_2 compounds. Furthermore, by extending their study up to 40 GPa, they demonstrated that if BaF_2 does undergo a subsequent insulator-metal transition, the later work of Kanchana *et al.*[6] which predicted a metallization pressure of 33 GPa was certainly an underestimate. Table I summarizes the structural details of the three observed phases of BaF_2 for various pressures at ambient temperature.

The work of Leger *et al.*[5] has been influential as it has served as the archetype for the cotunnite→Ni_2In structural progression in a number of experimental and computational studies on AX_2 compounds. This has been of particular importance, for example, in the case of recent experimental work on the heavy alkaline-earth hydrides[14–17] which adopt the cotunnite structure at ambient conditions and subsequently transform to the Ni_2In structure upon increasing pressure. In these instances, powder x-ray diffraction measurements alone were not sufficient to locate the position of hydrogen. Similarly, it has been important in computational works (see, for example, that on Li_2O) (Ref. 18), where proposed transition pressures approach or exceed the limits of routine static pressure experiments.

A close examination of Ref. 5, however, reveals some difficulties with the proposed Ni_2In structure. Specifically, the cotunnite structure is such that throughout the stable pressure regime, the a axis should be substantially more

TABLE I. Summary of the known structures of BaF_2 at ambient temperature. The refined x and z coordinates of the cotunnite phase are from data obtained at 7.9 GPa.

Type	Symmetry	Space group	Z-value	Atom	Wycoff site	x	y	z	Stability range (GPa)
Cubic fluorite	Cubic	$Fm3\text{-}m$	4	Ba^{2+}	4*a*	0	0	0	0–3
				F^{1-}	8*c*	1/4	1/4	1/4	
Cotunnite	Orthorhombic	*Pnma*	4	Ba^{2+}	4*c*	0.246(2)	1/4	0.119(1)	3–14
				F^{1-}	4*c*	0.370(3)	1/4	0.415(4)	
				F^{1-}	4*c*	0.987(5)	1/4	0.705(3)	
Ni_2In	Hexagonal	$P6_3/mmc$	2	Ba^{2+}	2*c*	1/3	2/3	1/4	14–77+
				F^{1-}	2*a*	0	0	0	
				F^{1-}	2*d*	1/3	2/3	3/4	

compressible than the b and c axes, which is precisely what was observed. Similarly, upon transformation to the Ni_2In structure, the c axis should be more compressible than the a axis (due to the close relationship between the two respective structures), resulting in a decreasing c/a ratio with increasing pressure. The *opposite* pressure dependence was observed. Furthermore, the observed relative diffraction intensities for the Ni_2In phase differ significantly from those expected based on the proposed structure; the observed differences can only be accounted for by severe or essentially total preferred orientation. Finally, there has been no subsequent account of complimentary experimental techniques to corroborate the proposed structure. With the above in mind, it is expedient to revisit the pressure-dependent structural progression of BaF_2.

The following work presents angle-dispersive powder x-ray diffraction and Raman spectroscopy experiments, together with first-principles calculations, in an effort to resolve the aforementioned difficulties. In the case of the diffraction experiments, samples were prepared both with and without a pressure-transmitting medium; the respective experiments revealed marked differences. In the absence of a pressure-transmitting medium, the x-ray diffraction results reproduced well the results (including the difficulties mentioned above) reported in Ref. 5. Conversely, with the use of helium as a pressure-transmitting medium, the pressure dependence of the lattice parameters evolved in accord with that expected for the Ni_2In structure, viz., the c/a ratio decreased with increasing pressure. Also, the observed relative intensities were more consistent with those expected from the structural model. Furthermore, subtle precursor phenomena proposed by Kunc *et al.*[18] were observed for the cotunnite structure at pressures just below the Ni_2In transition. The Raman spectroscopy results further corroborate the Ni_2In structure, as the two expected Raman-active modes were observed. Finally, our observations indicate that BaF_2 remains an insulator up to at least 77 GPa—the maximum experimental pressure attained in this study—and if a possible insulator-metal transition occurs in the same manner as observed for BaH_2 (Ref. 15), calculations suggest it is not expected to take place well into the megabar regime.

II. EXPERIMENTAL AND THEORETICAL DETAILS

Three separate samples were prepared from the same bulk powder sample of BaF_2 (Sigma-Aldrich, 99.999% trace metals analysis). Membrane-type diamond-anvil cells with 300 μm flat culet anvils were used. Rhenium gaskets with an initial thickness of 250 μm were preindented to 45–70 μm, after which compression chambers 75–125 μm in diameter were drilled using electric spark erosion. Two of the three samples were loaded without a pressure-transmitting medium. For the first sample, the primary objective was to collect diffraction data up to the highest pressure possible (perhaps as high as 100 GPa) in an effort to find the proposed insulator-metal transition. It should be noted that pressure-transmitting media (with the exception of helium or similarly hydrogen) offer marginal benefit at such high pressures and can complicate the diffraction data with unwanted x-ray scattering. For the second sample, the primary objective was to collect unambiguous Raman spectra to corroborate the Ni_2In structure, consequently no pressure-transmitting medium was used (at the expense of not obtaining the pressure dependence of the Raman-active modes under hydrostatic conditions). The third sample was loaded with helium using a high-pressure gas loading system available at the BL10XU beamline at SPring-8. We here note that although the sample cannot be characterized as truly hydrostatic upon solidification of the helium pressure-transmitting medium, we hereafter refer to this sample and the corresponding experimental results as hydrostatic. In each sample, a single ruby microsphere was placed in the compression chamber prior to loading and pressure measurements were carried out using ruby luminescence, $P=A/B[(\lambda/\lambda_0)^B-1]$, selecting appropriate parameters for pressure calculations based on the use (or lack) of a pressure-transmitting medium ($A=1904$ GPa with $B=5$ for nonhydrostatic conditions[19] and $B=7.665$ for hydrostatic conditions).[20]

Two separate angle-dispersive powder x-ray diffraction experiments were performed using synchrotron radiation. The first was carried out at the HXMA beamline at the CLS (Ref. 21) on one of the samples loaded without a pressure-transmitting medium. An incident wavelength of 0.515 96 Å

was selected using the Si (111) crystals of a fixed-exit double-crystal monochromator. Beamline optics were used for collimating and focusing the white beam and monochromatic radiation, respectively, and a final beam size of 30 $\times 30$ μm^2 was defined using a square-aperture tungsten carbide collimator. Powder x-ray diffraction images were captured on a Marresearch mar345 imaging plate detector (scanned at 100 μm pixel resolution) located 271.71(2) mm from the sample. The sample-to-detector distance was determined using x-ray diffraction images of silicon (National Institute of Standards and Technology, Standard Reference Material 640c), and research samples were located at the same position as the standard using a centering technique based on the x-ray transmission of the gasket.[22] During a typical exposure of 8 min, the sample was rocked over 6° to minimize detector saturation and to improve the intensity distribution along Debye rings.[22] Starting at ambient pressure, images were collected upon increasing pressure up to a maximum pressure of 77.1 GPa.

The second diffraction experiment was carried out at the BL10XU beamline at SPring-8 (Ref. 23) on the sample loaded with helium as a pressure-transmitting medium. A wavelength of 0.352 69 Å was selected using the diamond (111) crystals of a double-crystal monochromator. The x-ray beam was focused using glassy carbon compound refractive lenses (CRL) followed by another CRL made of an SU-8 polymer (an epoxy-based negative photoresist) providing a final beam spot 20×20 μm^2 at the sample. Powder x-ray diffraction images were captured on a Rigaku R-Axis IV imaging plate detector (scanned at 100 μm pixel resolution) located 307.74(2) mm from the sample. The sample-to-detector distance was determined using powder x-ray diffraction images of CeO_2, and research samples were located at the same position as the standard using automated microscopy. During a typical exposure of 10 min, samples were rocked over 10°. Starting at 0.7 GPa, images were collected upon increasing pressure up to a maximum pressure of 32.7 GPa.

All powder x-ray diffraction images were processed and integrated using FIT2D (Ref. 24) to obtain x-ray diffraction patterns of intensity vs 2θ. XRDA (Ref. 25) was used for pattern analysis and indexing. Whole-pattern refinements were performed on all patterns using FULLPROF.[26] Due to several complicating factors (see Sec. III A for more details), the Le Bail method of profile matching was applied to diffraction patterns of the high-pressure phases collected from the sample without a pressure-transmitting medium. Refined parameters included background, scale, lattice parameters, and pseudo-Voigt peak profile parameters. Rietveld refinements were carried out on all other patterns. Additional refined parameters included an overall isotropic displacement parameter, a Rietveld-Toraya correction for preferred orientation for the high-pressure phases, and fractional atomic coordinates for the cotunnite structure.

Raman spectroscopy measurements were performed on the two samples loaded without a pressure-transmitting medium. Spectra were collected from the same sample used in the diffraction experiment (starting at the maximum pressure of 77.1 GPa) upon decreasing pressure down to ambient pressure. For the second sample, spectra were collected from 0.3 GPa upon increasing pressure up to 31.5 GPa. Raman spectra were collected in near-backscattering geometry using a Jobin-Yvon S3000 triple-grating subtractive spectrograph equipped with a nitrogen-cooled charge-coupled device (CCD) detector. The 488 nm line of an Ar ion laser was used for excitation. All diffraction and spectroscopy experiments were carried out at ambient temperature.

First-principles calculations of the electronic structure were performed using the software package VASP.[27] Perdew-Becke-Erhenzof (PBE) projected augmented potentials (PAW) (Ref. 28) were used in all calculations. The $5s^25p^66s^2$ electrons of Ba were treated as valence. Monkhorst-Pack k meshes[29] of $10 \times 8 \times 12$, $12 \times 12 \times 8$, and $8 \times 8 \times 12$ were used for the cotunnite, Ni_2In, and AlB_2 structures, respectively. The unit-cell size (and fractional atomic coordinates, in the case of the cotunnite structure) was optimized for selected volumes, and the corresponding pressures were calculated directly from the stress tensor. In all cases, the plane-wave energy cutoff was set at 875 eV. The convergence criterion for energy calculations was 10^{-7} eV and for geometry optimizations, the residual forces on the atoms were smaller than 1.0×10^{-3} eV/Å. Phonon frequencies and eigenvectors for the Ni_2In phase were obtained using the ABINIT code[30] using the generalized gradient approximation[28] employing the pseudopotential plane-wave density-functional method on $8 \times 8 \times 8$ Monkhorst-Pack k meshes.[29] Troullier-Martins pseudopotentials[31] were employed for the phonon calculations treating the $6s^2$ electrons as valence. Equations of state data were obtained with Troullier-Martins and Hartswigsen-Goedecker-Hutter pseudopotentials[32] treating $6s^2$ and $5s^25p^66s^2$ electrons of Ba as valence, respectively.

III. RESULTS AND ANALYSIS

A. Powder x-ray diffraction

An x-ray diffraction image was first obtained from BaF_2 at ambient pressure and temperature conditions. The resulting pattern revealed no signs of impurity; the refined lattice parameter of the cubic fluorite structure was $a = 6.197\,7(5)$ Å consistent with previous measurements.[8] Figure 1 shows representative whole-pattern refinements from each of the three phases (cubic fluorite, cotunnite, and Ni_2In structures) from the nonhydrostatic (left) and hydrostatic (right) diffraction experiments. As expected, the characteristic features of the respective experiments showed marked contrast. The diffraction patterns of the high-pressure phases obtained from the nonhydrostatic sample exhibited substantial strain broadening as compared to those obtained from the hydrostatic sample (compare, for example, the resolution of closely spaced peaks at even modest 2θ values). Similarly, the nonhydrostatic experiment suffered from severe preferred orientation, as evidenced by the remarkable differences in relative intensities for the Ni_2In phase. Perhaps less expected was the nature of the pressure-induced phase transitions. In the nonhydrostatic case, the phase transitions were distinct and complete. The patterns obtained at 5.2 and 18.5 GPa (the first pressure points above the expected transition pressures of approximately 3 and 14 GPa) exhibited

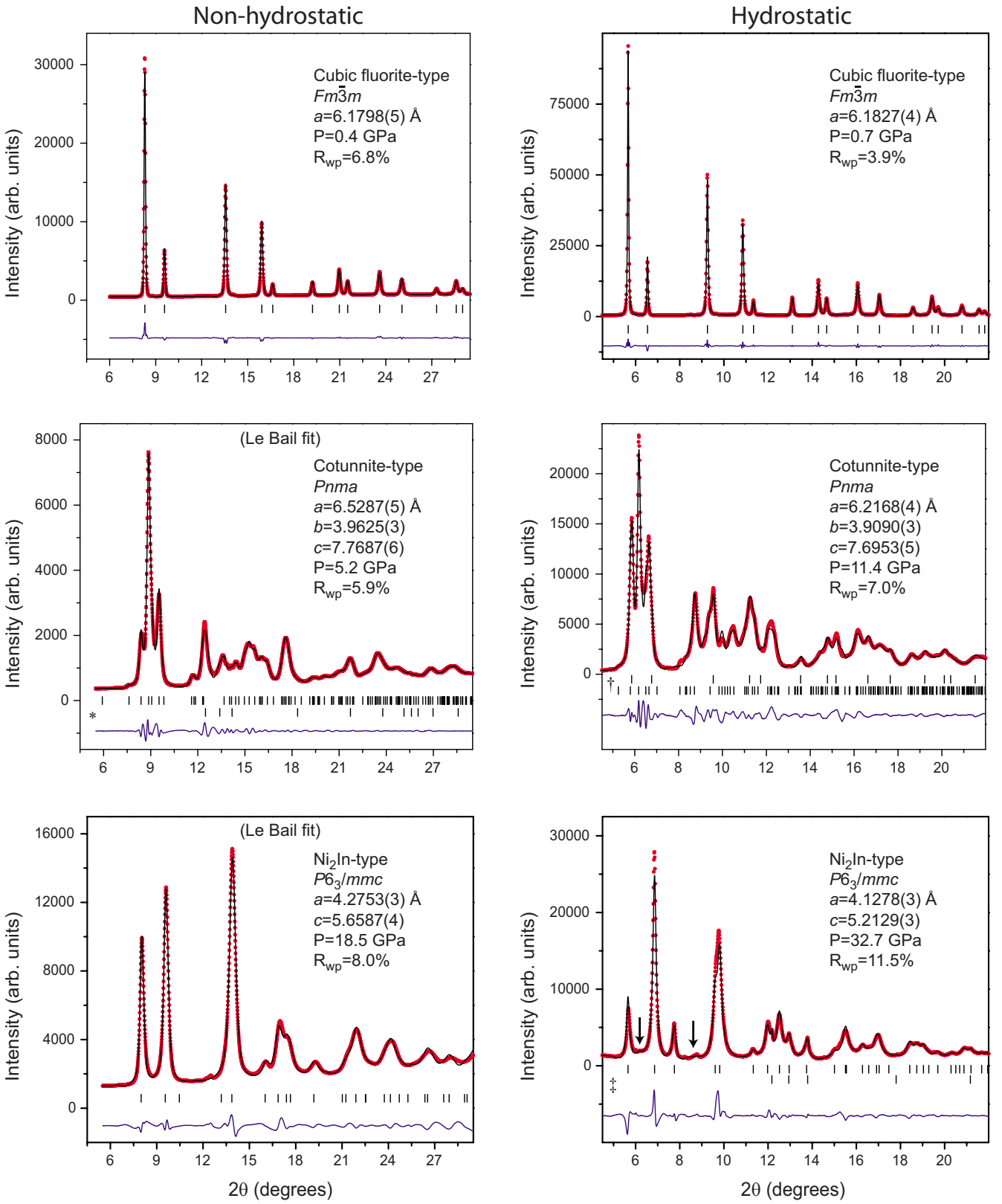

FIG. 1. (Color online) Representative Rietveld (or Le Bail, where indicated) refinements for the three observed phases of BaF_2 from the nonhydrostatic (left) and hydrostatic (right) powder x-ray diffraction experiments. Each plot includes the observed diffraction intensity (symbols), corresponding fit (solid line), expected Bragg peaks (vertical bars), and difference (bottom solid line). Additional Bragg peaks account for the scattering from the rhenium gasket (∗), the persistent cubic fluorite phase (†), or solid helium (‡). Trace amounts of the persistent cotunnite phase are indicated by arrows (bottom right). Note that the background has been subtracted from the plots obtained under hydrostatic conditions (right) to facilitate comparison against the expected Bragg peaks.

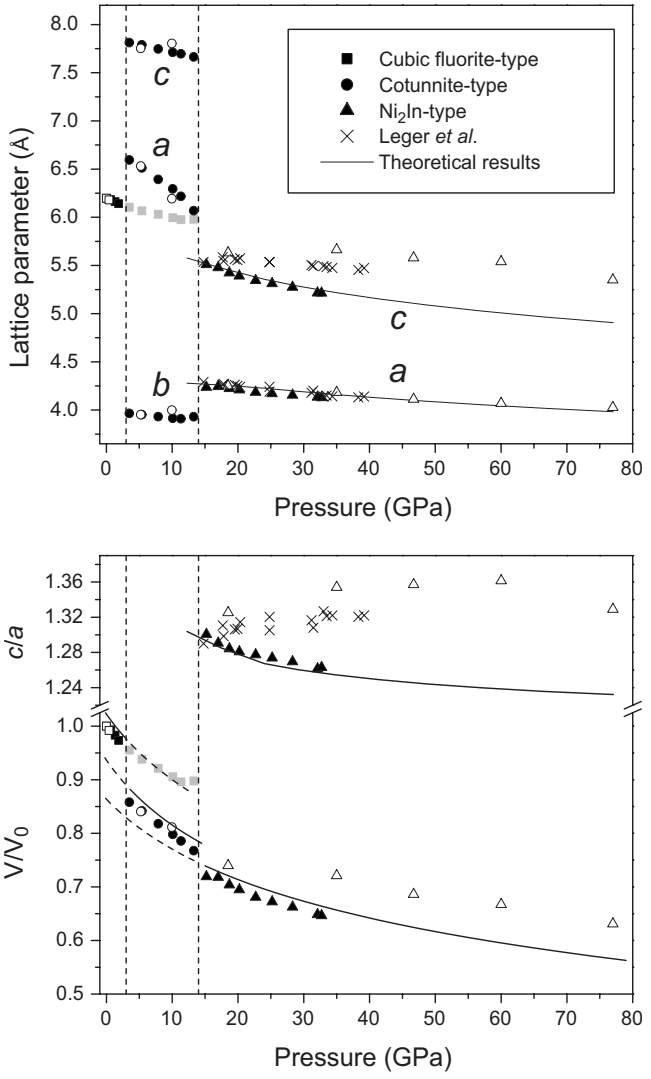

FIG. 2. Pressure dependence of the lattice parameters (top) and relative volume (bottom) for each of the three phases, as well as the c/a axial ratio for the Ni_2In phase (bottom). Open and closed symbols denote data from the nonhydrostatic and hydrostatic diffraction experiments, respectively. The gray squares represent the refined lattice parameter for the persistent cubic fluorite phase in the stable pressure regime of the cotunnite phase for the hydrostatic experiment.

peaks only from the cotunnite and Ni_2In structures, respectively. Conversely, in the case of the hydrostatic experiment, the phase transitions were extremely sluggish. The first (trace) sign of the cotunnite phase appeared at approximately 2 GPa but did not constitute the majority phase (based on quantitative analysis) until approximately 5.5 GPa, and the cubic fluorite phase persisted as a minority phase up to at least 13 GPa, nearing the onset of the cotunnite $\rightarrow Ni_2In$ phase transition. Similarly, trace amounts of the cotunnite phase persisted throughout the stable pressure regime of the Ni_2In phase up to the maximum sample pressure of 32.7 GPa. As further discussed below, this introduced complications with carrying out structural refinements and with obtaining accurate experimental equations of state.

1. Cubic fluorite phase

The cubic fluorite phase was stable up to approximately 3 GPa. Full structural refinements were carried out on patterns from both the nonhydrostatic and hydrostatic experiments, as shown in Fig. 1 (top). Figure 2 shows the refined lattice parameters and relative volume for each of the three phases, together with the results of the first-principles calculations. While the narrow pressure range and correspondingly small volume compression of the pure cubic fluorite phase precluded obtaining a meaningful experimental equation of state, the data nevertheless agree well with the equation of state obtained by fitting the results of the first-principles calculations to a third-order Birch-Murnaghan equation of state. The resulting isothermal bulk modulus $B_0=58.2(3)$ GPa is in good agreement with that obtained from ultrasonic measurements obtained at ambient pressure.[33] See Table II for complete experimental and theoretical equation of state parameters for all phases.

2. Cotunnite phase

Above approximately 3 GPa, a pressure-induced phase transition was indicated by the marked change in the x-ray diffraction images. Indexing the orthorhombic cotunnite phase was straightforward for patterns from both of the diffraction experiments. Note that here the indexing is consistent with the *Pnma* permutation (as opposed to *Pnam* per-

TABLE II. Equation of state parameters for the three phases of BaF_2 obtained by fitting $P(V)$ data to a third-order Birch-Murnaghan equation of state. $V_0=59.52(1)$ Å^3/BaF_2 based on the x-ray diffraction data obtained at ambient conditions.

	Expt.			Theor.		
	B_0 (GPa)	B_0'	V/V_0	B_0 (GPa)	B_0'	V/V_0
Fluorite	57[a]	n/a	n/a	58.2(3)	4.67(2)	1.022(1)
Cotunnite	51(4)	4.7[b]	0.92(1)	52(1)	4.7(3)	0.937(1)
Ni_2In	56(5)	4.67[b]	0.86(2)	69(1)	4.67(2)	0.864(2)

[a]Reference 33.
[b]Assumed, based on theoretical results.

mutation used in Refs. 10 and 5; for a detailed discussion on the various permutations of the *Pnma* space group, see Hybler's work[34] with regard to α-$PbCl_2$). As shown in Fig. 2 (top), there is a marked difference in the pressure dependence among the various lattice parameters. Specifically, the a axis is much more compressible than the b and c axes, decreasing by approximately 0.046 Å/GPa as compared to 0.008 and 0.016 Å/GPa, respectively. Despite the relatively narrow stable pressure regime for the cotunnite phase, the experimental data were fit to a third-order Birch-Murnaghan equation of state, yielding an isothermal bulk modulus B_0 =51(4) GPa (B_0' fixed at 4.7, the value obtained from the theoretical calculations). This result is less than 79(10) GPa reported in Ref. 5, however, the underestimate here is likely due to the coexistence of the cubic fluorite and cotunnite phases. A volume collapse of approximately 10% was observed at the transition pressure of 3 GPa.

Of the three stable structures of BaF_2 studied in this work, the cotunnite structure is the only one for which the atoms are not located in special positions. Specifically, each of the three atoms in the asymmetric unit occupies the 4c position, with only the y coordinate constrained by symmetry. Unfortunately, the preferred orientation present in the nonhydrostatic experiment precluded a full structural refinement, as ambiguity was introduced by the strong correlation between the degree/direction of the preferred orientation and the fractional x and z coordinates of the respective atoms. Similarly, the coexistence of phases in the hydrostatic experiment does not rule out ambiguity in the refined atomic positions. Nevertheless, to obtain full structural refinements, the atomic positions obtained from the first-principles calculations were initially used. These atomic positions are in excellent agreement with the refined positions reported in Ref. 5. Table I includes the refined atomic positions for data obtained at 7.9 GPa. Figure 1 (middle) shows representative Le Bail and Rietveld refinements for the nonhydrostatic and hydrostatic experiments, respectively.

In their first-principles investigation of Li_2O, Kunc *et al.*[18] suggested precursor phenomena that accompany the cotunnite $\rightarrow Ni_2In$ transition. At ambient conditions, Li_2O adopts the cubic antifluorite structure and undergoes a pressure-induced structural phase transition to the anticotunnite structure at approximately 50 GPa (Ref. 35). (Note the antiphase nomenclature refers to A_2X, as opposed to AX_2, compounds.) Their computational results suggested that Li_2O will subsequently transform to the Ni_2In structure at approximately 135 GPa, with precursor phenomena to the phase transition characterized by distinct nonlinearities in the c/b and a/b axial ratios (the latter more so than the former) of the anticotunnite structure. Interestingly, they specifically suggested that BaF_2 would serve as a good candidate to explore these phenomena experimentally. Figure 3 (top) shows these axial ratios for the cotunnite phase of BaF_2 (from the hydrostatic experiment) over the stable pressure range of 3–14 GPa, which exhibit the proposed nonlinearities. Furthermore, as shown in Fig. 3 (bottom), these nonlinearities are the result of a sharp decrease in a, together with a slight *increase* in b, just before the phase transition—precisely as suggested in Ref. 18.

To summarize the x-ray diffraction results for the cubic fluorite and cotunnite phases, the results of the nonhydrostatic and hydrostatic experiments—as well as the results of the first-principles calculations—are essentially in agreement, and moreover, are in general agreement with the results of Ref. 5. We here add to the description the precursor phenomena for the cotunnite phase just prior to transforming to the Ni_2In structure. It is upon transforming to the Ni_2In structure that the various results begin to show marked differences.

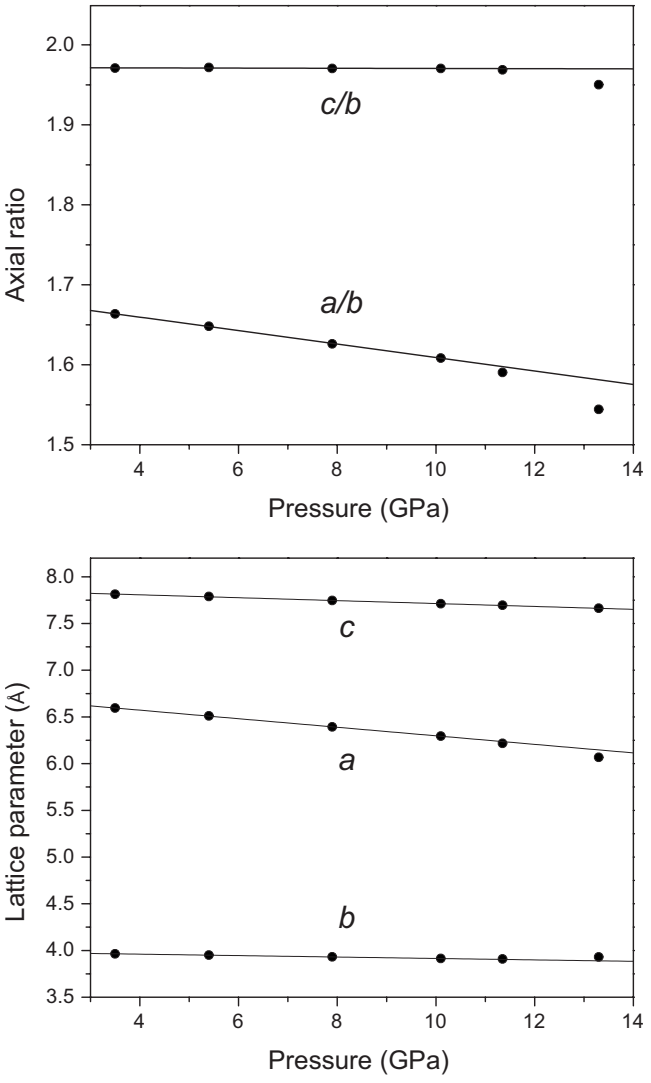

FIG. 3. Pressure dependence of the axial ratios (top) and lattice parameters (bottom) of the cotunnite phase from the hydrostatic experiment, detailing the precursor phenomena observed just prior to the Ni_2In transformation. The solid lines represent linear fits obtained from the first four data points of the respective ratios or lattice parameters.

3. Ni_2In *phase*

Above approximately 14 GPa, a subsequent phase transition was observed, indicated again by distinct changes in the x-ray diffraction images. The resulting x-ray diffraction patterns were readily indexed to a hexagonal unit cell. As shown in Fig. 2 (top), there was excellent agreement for the refined values of the a axis among the nonhydrostatic and hydro-

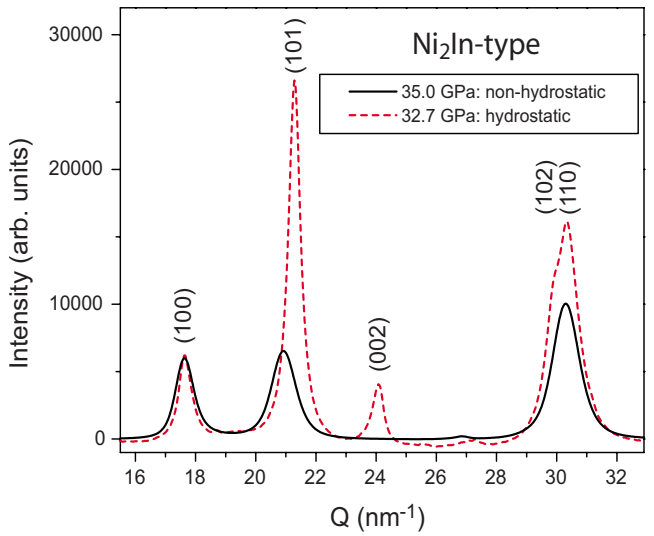

FIG. 4. (Color online) A comparison of x-ray diffraction patterns of the Ni_2In phase from the nonhydrostatic and hydrostatic diffraction experiments reveals marked differences in intensity and line position due to severe preferred orientation and atypical axial compression.

static experiments, the results of Ref. 5, and the theoretical results. The same cannot be said about the c axis. A significantly larger c axis was observed in the nonhydrostatic experiment and (to a lesser extent) in Ref. 5, as compared to the hydrostatic and theoretical results. Furthermore, the former two showed an increase in the c/a ratio with increasing pressure, while the latter two showed the opposite pressure dependence. As already discussed, the close relationship between the high-pressure structures suggests that the highly compressible a axis in the cotunnite structure should in turn result in a highly compressible c axis in the Ni_2In structure.

These observed differences can be accounted for by preferred orientation. With the c axis of the Ni_2In phase normal to the load axis—and consequently the incident x-ray beam—the $(00l)$ reflections would be absent, and (hkl) reflections with $l \neq 0$ would show marked decreases in intensity. Furthermore, upon compression along the load axis of the cell, the compression along the a axis would be close to what would be observed even under hydrostatic conditions, while the compression along c would be minimized due to the orientation of the crystallites. This is well illustrated in Fig. 4, which compares intensities over a selected region of Q space from the nonhydrostatic and hydrostatic experiments at approximately the same pressure, viz., 35.0 and 32.7 GPa, respectively. It is important to note that the background has been subtracted from the pattern obtained under hydrostatic conditions, and a small Q shift in the nonhydrostatic experiment of 0.15 nm^{-1} (equivalent to 0.07° 2θ) has been applied to aid in comparing peak positions; however, no intensity scaling has been applied to either pattern. The intensities of the (100) reflection [i.e., an $(hk0)$ plane] are in excellent agreement. However, the (101) reflection shows extreme differences in intensity and position due to preferred orientation and minimized compression along the c axis, respectively. The effect on intensities is most extreme in the case of the (002) peak [i.e., a $(00l)$ peak], which is completely absent in the nonhydrostatic case.

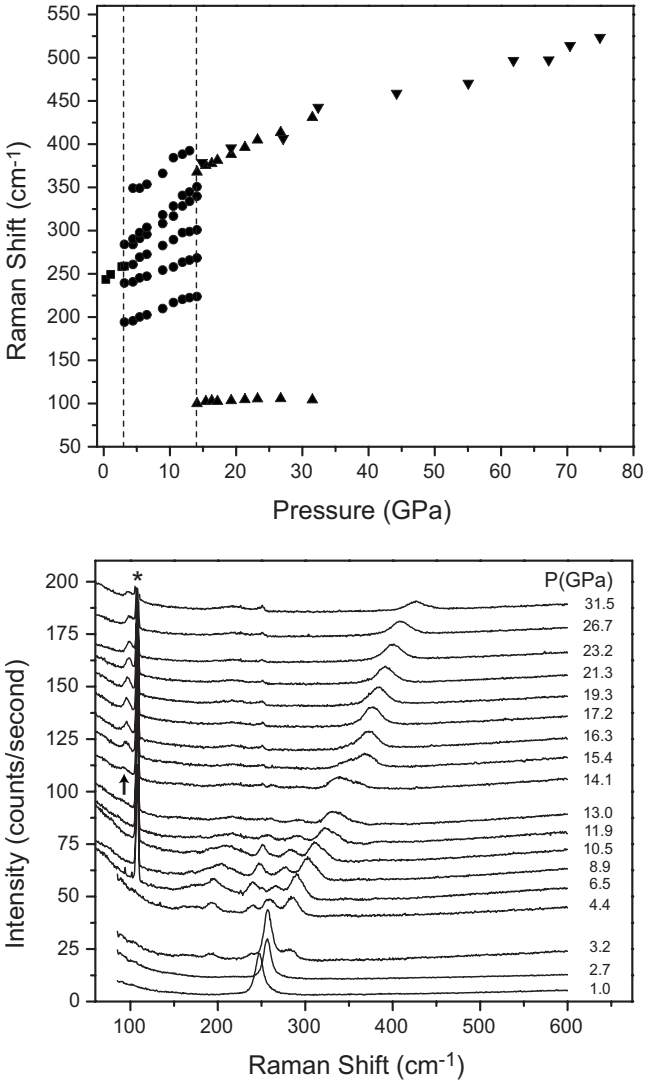

FIG. 5. The pressure dependence of the observed Raman modes (top) and several Raman spectra obtained upon increasing pressure (bottom). The inverted triangles represent data collected upon decreasing pressure; all other data were collected upon increasing pressure. The arrow indicates the first sign of the low-wave-number mode associated with the Ni_2In phase. The intense narrow peak at approximately 105 cm^{-1} (*) arises from stray light associated with collecting spectra from very low wave numbers (its position remains constant with pressure). For clarity, the intensity of the bottom two spectra has been halved and a vertical offset has been added to all spectra.

The pressure-dependent volume of the Ni_2In phase was fit to a third-order Birch-Murnaghan equation of state, yielding B_0=58(5) GPa (B_0' fixed at 4.67, the value obtained from the theoretical calculations). Again, this is likely an underestimation due to the coexistence with the cotunnite phase up to the maximum pressure of the study. But nevertheless, it is clear after measuring the compression under the best possible hydrostatic conditions that the Ni_2In phase of BaF_2 is much more compressible than previously reported. The volume collapse at the transition pressure of 14 GPa was approximately 5%.

B. Raman spectroscopy

The primary purpose of the Raman experiments was to corroborate the proposed Ni_2In structure of BaF_2. A group theoretical analysis indicates that only two modes should be observed, according to the irreducible representation $\Gamma_{\text{Raman}}=2E_g$. Similarly, for the cubic fluorite and cotunnite phases, the irreducible representations of the Raman-active modes are $\Gamma_{\text{Raman}}=T_{2g}$ (a single mode) and $\Gamma_{\text{Raman}}=6A_g+3B_{1g}+6B_{2g}+3B_{3g}$ (18 modes), respectively. Figure 5 shows the pressure dependence of the observed Raman modes from the two nonhydrostatic samples (top), together with several Raman spectra from the experiment taken upon increasing pressure (bottom). Considering first the data taken upon increasing pressure, at ambient pressure the spectrum exhibited a single peak at 240 cm^{-1}. The peak shifted to higher wave numbers with increasing pressure at a rate of just over 8 cm^{-1}/GPa, in excellent agreement with that observed in Ref. 11. At 3.2 GPa, the peak intensity fell sharply and several broad peaks appeared on either side, indicating the onset of the transition to the cotunnite structure. Given the experiment was carried out at ambient temperature, it was not possible to resolve the many peaks in the 150–300 cm^{-1} range, and furthermore, many of the modes observed by Kessler *et al.*[11] at lower wave numbers were not observed. Nevertheless, the broad multimode band at ~200 cm^{-1}, together with the triplet in the 225–300 cm^{-1} range, was consistent with the previous study. The pressure dependence of these modes over the stable pressure regime ranged from approximately 3–6 cm^{-1}/GPa, in agreement with that observed for α-PbF_2 (Ref. 11). Above 10 GPa, the intensity of the peaks again decreased significantly, and an asymmetry of the doublet at approximately 325 cm^{-1} developed, with a small shoulder emerging on the high-wave-number side. These developments may constitute the Raman manifestation of the precursor phenomena observed in the x-ray diffraction experiments. At 14.1 GPa, a weak peak emerged at approximately 95 cm^{-1} (indicated by the arrow in Fig. 4, bottom) and the weak shoulder of the peak at 325 cm^{-1} became dominant. Above 16 GPa, the phase transition was complete and the two peaks remained the only Raman features in the spectra up to the maximum pressure of 31.5 GPa. First-principles calculations of the two expected Raman modes for the Ni_2In phase at 40 GPa yielded expected frequencies of 115 and 590 cm^{-1}. While these calculated frequencies are higher than the observed values, the general range is nevertheless consistent with what was observed experimentally.

For the next sample studied upon decreasing pressure (the same as that used in the nonhydrostatic diffraction experiment), at 77.1 GPa, the spectrum had a single, weak, and broad peak at approximately 525 cm^{-1}. The peak shifted to lower wave numbers with decreasing pressure; however, due to the poor signal-to-background ratio and the breadth of the peak, it was difficult to obtain a satisfactory fit for the peak, hence the observed scatter in the data. However, the observed peak was consistent with the high-wave number peak observed for the Ni_2In phase in the companion experiment. The low-wave-number peak was not observed, however. Below 5 GPa, the group of peaks characteristic of the cotunnite phase emerged about this single peak. The group remained down to ambient pressure, and the peak associated with the cubic fluorite phase emerged, indicating a mixture of phases.

IV. DISCUSSION

As mentioned in Sec. I, a computational study predicted metallization of BaF_2 at 33 GPa (Ref. 6); however, it had already been demonstrated by Leger *et al.* that the Ni_2In phase was stable, and the sampled remained completely transparent to visible light, up to at least 40 GPa. More recently, *in situ* conductivity measurements on BaF_2 were carried out by Hao *et al.*[7] up to a pressure of approximately 60 GPa. While no metallization was observed, it was suggested that BaF_2 could be characterized as a wide-gap semiconductor at pressures above 25 GPa (with a band gap of approximately 1.2 eV) and based on extrapolation of the measured band gap as a function of pressure, metallization (zero band gap) would occur at approximately 87 GPa. However, no conclusion was made as to whether this would be accompanied by a first-order structural phase transition.

A high-pressure powder x-ray diffraction study of BaH_2 by Kinoshita *et al.*[15] was the first to report a post-Ni_2In structure for an ionic AX_2 compound. Specifically, the onset of the pressure-induced structural phase transition appeared at approximately 50 GPa, with the phase transformation completed at approximately 65 GPa, and furthermore the transition was reversible (however, large hysteresis was observed). The AlB_2 structure (hexagonal, $P6/mmm$) was proposed for the post-Ni_2In phase. The authors' unpublished research of BaH_2 agrees with Kinoshita *et al.*, and we here add to the characterization of the high-pressure phase by noting that upon transforming to the AlB_2 structure, the band gap is narrow enough that the sample is no longer transparent to visible light. It is reasonable to suggest that if BaF_2 is to undergo a subsequent structural phase transition, it might be characterized by the same structure as BaH_2. However, the current study demonstrates that the Ni_2In structure remains stable up to at least 77 GPa, and furthermore the sample remains transparent to visible light, viz., the band gap must still be significantly larger than 1 eV. We thus conclude that BaF_2 does not transform to a metallic state up to the maximum pressure reached in this study.

A linear relationship between the molar volume and the cube of the mean cation-anion distance has been established for several ionic AX_2 compounds: both at ambient- and high-pressure conditions (see, for example, Refs. 1 and 5). Specifically, $V_{\text{molar}}=kd_0^3/N$, where $k=14.4(6)$, d_0 is the mean cation-anion distance, and N is the cation coordination number. It has been shown for CaH_2 and BaH_2 that the relationship holds not only at ambient pressure and immediately following a pressure-induced phase transition, but also throughout the stable pressure range of a given phase.[17] Figure 6 shows this relationship also holds for each of the three phases of BaF_2 throughout the respective stable pressure ranges. Notably, the relationship suggests that the ionic nature of the bonding is maintained up to the maximum pressure of 77.1 GPa; further suggesting that BaF_2 remains an insulator.

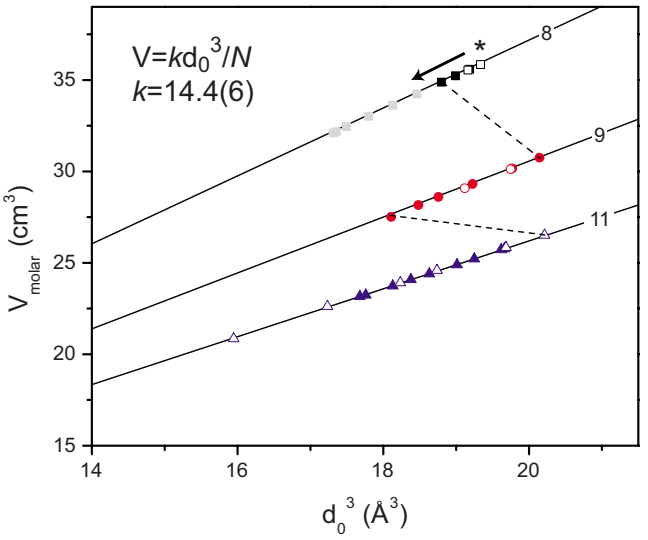

FIG. 6. (Color online) Molar volume vs the cube of the mean cation-anion distance for 8-, 9-, and 11-coordinated Ba^{2+}. Open and closed symbols denote data from the nonhydrostatic and hydrostatic diffraction experiments, respectively. The asterisk (*) indicates ambient pressure. Upon increasing pressure, data tend toward the origin, or in the case of a phase transition, increase in coordination number (as well as mean cation-anion distance) as indicated by the dotted lines. The relationship holds throughout the stable pressure regimes of the respective phases, up to the maximum pressure of the study (77.1 GPa), indicating that the bonding remains characteristically ionic.

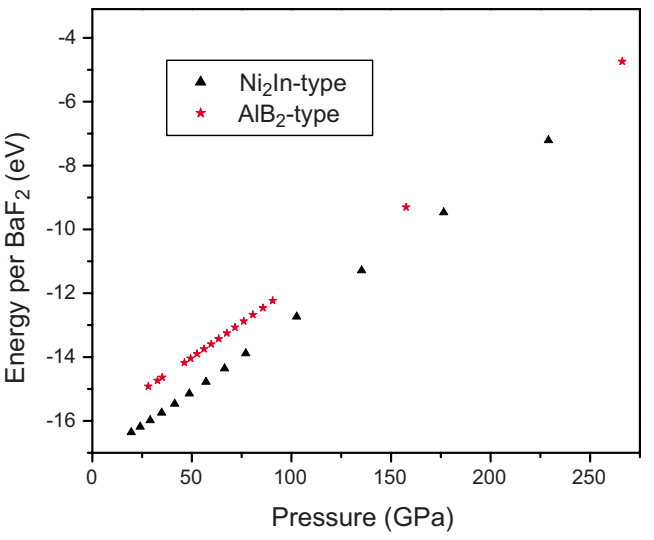

FIG. 7. (Color online) The calculated energy vs pressure for the observed Ni_2In structure and hypothetical AlB_2 structure of BaF_2 suggest that BaF_2 does not undergo an insulator-metal transition analogous to that observed for BaH_2.

Figure 7 shows a comparison of the calculated energy vs pressure for the observed Ni_2In phase and the hypothetical high-pressure AlB_2 phase for BaF_2. The results clearly show a transition to the AlB_2 structure as observed for BaH_2 is not expected to occur for BaF_2 up to at least 250 GPa. Furthermore, our calculations of the band gap suggest that the Ni_2In phase remains insulating at pressures greater than 500 GPa. In short, if BaF_2 does undergo a subsequent pressure-induced phase transition, it is either at pressures which exceed current experimental static pressure limits or it is characterized by a different structure than that observed for BaH_2.

Difficulties arising from nonhydrostatic pressure conditions, such as anisotropic strain broadening and preferred orientation, are frequently encountered. As hexagonal structures are particularly prone to texture, it is not necessarily surprising that the nonhydrostatic and hydrostatic experiments exhibited marked contrast for the Ni_2In data (although the magnitude of the contrast is certainly surprising, e.g., a difference of almost 10% in the c axis at approximately 35 GPa). On the other hand, difficulties arising from hydrostatic pressure conditions are less frequently encountered; in this particular case, hydrostatic conditions gave rise to extremely sluggish pressure-induced phase transitions. As for a possible explanation, we here suggest that microscopic domains may be present in the sample, and these domains are preserved by the hydrostatic conditions. As a portion of the sample in a given domain transforms to a higher-density phase, the corresponding local volume collapse permits a portion of the sample in the same domain to persist in the lower-density phase. Conversely, the shear forces present under nonhydrostatic conditions are sufficient to break down the domain boundaries, resulting in distinct, complete phase transitions. The same result could likely be achieved in the hydrostatic case through annealing by means of laser heating or a conventional furnace. A more thorough exploration of phase coexistence over such a broad pressure range presents an opportunity for further study.

V. CONCLUSION

The primary purpose of the current work was to corroborate the proposed Ni_2In structure of BaF_2 for pressures above 14 GPa. Compression under nonhydrostatic conditions gave rise to atypical compression of the lattice parameters in the high-pressure phase, as well as poor agreement between observed and expected relative intensities due to preferred orientation. These difficulties were resolved by carrying out the experiment under the best possible hydrostatic conditions. The Raman experiments further support the proposed structure, as the spectra exhibited two Raman-active modes as expected for the Ni_2In phase. The previously proposed precursor phenomena accompanying the cotunnite $\rightarrow Ni_2In$ transition were clearly observed in the hydrostatic x-ray diffraction study and this may be further indicated by the marked decrease in intensity of the majority of the observed Raman modes prior to the Ni_2In transition. Finally, the Ni_2In phase of BaF_2 remained stable up to at least 77 GPa and no indications of metallization were observed. If BaF_2 is to undergo a subsequent pressure-induced phase transition in a manner similar to BaH_2, it is likely that this will not occur until well into the multimegabar regime, or alternatively, it will be characterized by a different crystal structure.

ACKNOWLEDGMENTS

Synchrotron-radiation experiments described in this work were performed in part at the Canadian Light Source, which is supported by NSERC, NRC, CIHR, and the University of Saskatchewan, and in part at the beamline BL10XU at SPring-8, with the approval of the Japan Synchrotron Radiation Research Institute (JASRI). S.D., J.S.T., and J.S. wish to acknowledge the financial support of NSERC.

*Author to whom correspondence should be addressed. jsmit068@uottawa.ca

†Present address: Lehrstuhl für Theoretische Chemie, Ruhr-Universität Bochum, 44780 Bochum, Germany.

[1] *Metal Oxides: Chemistry and Applications*, edited by J. L. G. Fierro (Taylor & Francis, Florida, 2006).

[2] L. G. Liu and W. A. Bassett, *Elements, Oxides, Silicates: High-Pressure Phases with Implications for the Earth's Interior* (Oxford University Press, New York, 1986).

[3] B. Sakintuna, F. Lamari-Darkrim, and M. Hirscher, Int. J. Hydrogen Energy **32**, 1121 (2007).

[4] D. Colognesi, G. Barrera, A. J. Ramirez-Cuesta, and M. Zoppi, J. Alloys Compd. **427**, 18 (2007).

[5] J. M. Leger, J. Haines, A. Atouf, O. Schulte, and S. Hull, Phys. Rev. B **52**, 13247 (1995).

[6] V. Kanchana, G. Vaitheeswaran, and M. Rajagopalan, J. Alloys Compd. **359**, 66 (2003).

[7] A. M. Hao, C. X. Gao, M. Li, C. Y. He, X. W. Huang, D. M. Zhang, C. L. Yu, G. T. Zou, Y. C. Li, X. D. Li, and J. Liu, Chin. Phys. Lett. **23**, 2917 (2006).

[8] A. H. Swanson and E. Tatge, Natl. Bur. Stand. Circ. (U. S.) **539**, 1 (1953).

[9] H. I. Smith and J. H. Chen, Bull. Am. Phys. Soc. **11**, 414 (1966).

[10] K. F. Seifert, Fortschr. Mineral. **45**, 214 (1967).

[11] J. R. Kessler, E. Monberg, and M. Nichol, J. Chem. Phys. **60**, 5057 (1974).

[12] J. M. Leger, J. Haines, and A. Atouf, Phys. Rev. B **51**, 3902 (1995); J. Appl. Crystallogr. **28**, 416 (1995); J. Phys. Chem. Solids **57**, 7 (1996).

[13] B. Lebech, N. H. Andersen, S. Steenstrup, and A. S. Pedersen, Acta Crystallogr., Sect. C: Cryst. Struc. Commun. **39**, 1475 (1983).

[14] K. Kinoshita, M. Nishimura, Y. Akahama, and H. Kawamura, Proceedings of 20th AIRAPT Conference, 2005 (unpublished).

[15] K. Kinoshita, M. Nishimura, Y. Akahama, and H. Kawamura, Solid State Commun. **141**, 69 (2007).

[16] J. S. Tse, D. D. Klug, S. Desgreniers, J. S. Smith, R. Flacau, Z. Liu, J. Hu, N. Chen, and D. T. Jiang, Phys. Rev. B **75**, 134108 (2007).

[17] J. S. Smith, S. Desgreniers, J. S. Tse, and D. D. Klug, J. Appl. Phys. **102**, 043520 (2007).

[18] K. Kunc, I. Loa, and K. Syassen, Phys. Rev. B **77**, 094110 (2008).

[19] H. K. Mao, P. M. Bell, J. W. Shaner, and D. J. Steinberg, J. Appl. Phys. **49**, 3276 (1978).

[20] H. K. Mao, J. A. Xu, and P. M. Bell, J. Geophys. Res. **91**, 4673 (1986).

[21] S. Desgreniers, J. S. Smith, J. S. Tse, C. Y. Kim, N. Chen, D. T. Jiang, and D. D. Klug, Canadian Light Source Activity Report 2007, p. 132 (unpublished).

[22] J. S. Smith and S. Desgreniers, J. Synchrotron Radiat. **16**, 83 (2009).

[23] Y. Ohishi, N. Hirao, N. Sata, K. Hirose, and M. Takata, High Press. Res. **28**, 163 (2008).

[24] A. P. Hammersley, S. O. Svensson, M. Hanfland, A. N. Fitch, and D. Häusermann, High Press. Res. **14**, 235 (1996).

[25] S. Desgreniers and K. Lagarec, J. Appl. Crystallogr. **27**, 432 (1994); **31**, 109 (1998).

[26] J. Rodriguez-Carvajal, Physica B **192**, 55 (1993).

[27] G. Kresse and J. Furthmuller, Comput. Mater. Sci. **6**, 15 (1996); Phys. Rev. B **54**, 11169 (1996).

[28] J. P. Perdew, K. Burke, and M. Ernzerhof, Phys. Rev. Lett. **77**, 3865 (1996).

[29] H. J. Monkhorst and J. D. Pack, Phys. Rev. B **13**, 5188 (1976).

[30] X. Gonze, Phys. Rev. B **55**, 10337 (1997); X. Gonze and C. Lee, *ibid.* **55**, 10355 (1997); X. Gonze *et al.*, Comput. Mater. Sci. **25**, 478 (2002).

[31] N. Troullier and J. L. Martins, Phys. Rev. B **43**, 1993 (1991).

[32] M. Krack, Theor. Chem. Acc. **114**, 145 (2005).

[33] C. Wong and D. E. Schuele, J. Phys. Chem. Solids **29**, 1309 (1968).

[34] J. Hybler, Cryst. Res. Technol. **23**, 1127 (1988).

[35] K. Kunc, I. Loa, A. Grzechnik, and K. Syassen, Phys. Status Solidi B **242**, 1857 (2005).